Biochemical Pharmacology xxx (2016) xxx–xxx

Contents lists available at ScienceDirect

Biochemical Pharmacology

journal homepage: www.elsevier.com/locate/biochempharm

Rational design of an AKR1C3-resistant analog of PR-104 for enzyme-prodrug therapy

Alexandra M. Mowday [a], Amir Ashoorzadeh [a], Elsie M. Williams [b,1], Janine N. Copp [b,2], Shevan Silva [a], Matthew R. Bull [a], Maria R. Abbattista [a], Robert F. Anderson [a,c], Jack U. Flanagan [a,c], Christopher P. Guise [a,c], David F. Ackerley [b,c], Jeff B. Smaill [a,c], Adam V. Patterson [a,c,*]

[a] Auckland Cancer Society Research Centre, School of Medical Sciences, The University of Auckland, Auckland 1023, New Zealand
[b] School of Biological Sciences, Victoria University of Wellington, Wellington 6140, New Zealand
[c] Maurice Wilkins Centre for Molecular Biodiscovery, School of Biological Sciences, The University of Auckland, Auckland 1023, New Zealand

ARTICLE INFO

Article history:
Received 25 May 2016
Accepted 20 July 2016
Available online xxxx

Chemical compounds studied in this article:
PR-104 (PubChem CID: 11455973)
PR-104A (PubChem CID: 9848786)
SN34037 (PubChem CID: 73671441)
SN34507 (PubChem CID: 90043967)
SN35539 (PubChem CID: 90043246)

Keywords:
Prodrug
Alkylation
Oxidoreductase
Aldo-keto reductase 1C3
Hypoxia

ABSTRACT

The clinical stage anti-cancer agent PR-104 has potential utility as a cytotoxic prodrug for exogenous bacterial nitroreductases expressed from replicating vector platforms. However substrate selectivity is compromised due to metabolism by the human one- and two-electron oxidoreductases cytochrome P450 oxidoreductase (POR) and aldo-keto reductase 1C3 (AKR1C3). Using rational drug design we developed a novel mono-nitro analog of PR-104A that is essentially free of this off-target activity *in vitro* and *in vivo*. Unlike PR-104A, there was no biologically relevant cytotoxicity in cells engineered to express AKR1C3 or POR, under aerobic or anoxic conditions, respectively. We screened this inert prodrug analog, SN34507, against a type I bacterial nitroreductase library and identified *E. coli* NfsA as an efficient bioactivator using a DNA damage response assay and recombinant enzyme kinetics. Expression of *E. coli* NfsA in human colorectal cancer cells led to selective cytotoxicity to SN34507 that was associated with cell cycle arrest and generated a robust 'bystander effect' at tissue-like cell densities when only 3% of cells were NfsA positive. Anti-tumor activity of SN35539, the phosphate pre-prodrug of SN34507, was established in 'mixed' tumors harboring a minority of NfsA-positive cells and demonstrated marked tumor control following heterogeneous suicide gene expression. These experiments demonstrate that off-target metabolism of PR-104 can be avoided and identify the suicide gene/prodrug partnership of *E. coli* NfsA/SN35539 as a promising combination for development in armed vectors.

1. Introduction

Gene-directed enzyme prodrug therapy (GDEPT) is an approach whereby cancer tropic vectors such as replication-competent viruses or bacteria are employed to deliver therapeutic genes to the tumor microenvironment. The exogenous gene typically introduces a new catalytic function into the tumor microenvironment that can confer conditional sensitivity to otherwise inert prodrugs [1]. The most widely studied nitroaromatic enzyme/prodrug combination for GDEPT is the nitroreductase (NTR) from *Escherichia coli*, NfsB, in combination with the prodrug CB1954 (5-(aziridin-1-yl)-2,4-dinitrobenzamide); see review [2] and references therein. Although efficacy was demonstrated with this combination in cell culture models [3,4] and tumor xenografts using replication-defective viruses [5,6], to date this combination has demonstrated limited utility in human clinical trials. Poor aqueous solubility of CB1954 [7], modest kinetics of CB1954 reduction by NfsB [8], and dose-limiting hepatotoxicity in humans [9] are thought to be possible reasons for the lack of efficacy observed.

The prodrug PR-104 (Fig. 1A), (2-((2-bromoethyl)(2-((2-hydroxyethyl)carbamoyl)-4,6-dinitrophenyl)amino) ethyl methanesulfonate phosphate ester) represents an alternative nitroaromatic substrate for NTRs. PR-104 is a water-soluble phosphate ester 'pre-prodrug' which undergoes facile conversion to the corresponding lipophilic alcohol PR-104A in plasma, and was initially designed and optimized as a hypoxia-activated prodrug (HAP) with

* Corresponding author at: Auckland Cancer Society Research Centre, School of Medical Sciences, The University of Auckland, Auckland 1023, New Zealand.
E-mail address: a.patterson@auckland.ac.nz (A.V. Patterson).
[1] Current address: Department of Chemistry, Emory University, 1515 Dickey Drive, Atlanta, Georgia, USA.
[2] Current address: Michael Smith Laboratories, University of British Columbia, Vancouver, BC, Canada.

http://dx.doi.org/10.1016/j.bcp.2016.07.015
0006-2952/

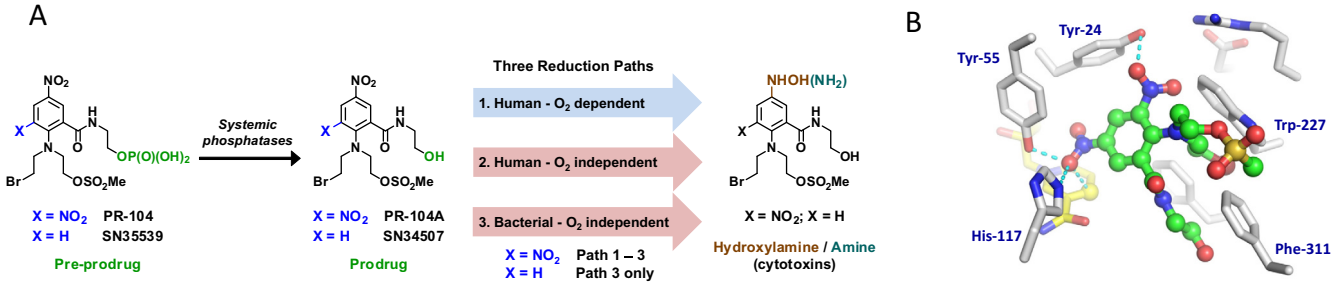

Fig. 1. Rationale for design of the prodrug SN34507: (A) Schematic of pre-prodrug PR-104 or SN35539 conversion to prodrug PR-104A and SN34507, respectively, with subsequent reduction to cytotoxic hydroxylamine or amine metabolites by up to three independent metabolic pathways; (B) Binding model of PR-104A in the active site of human aldo-keto reductase 1C3 indicating potential for hydrogen-bond formation between the *ortho* nitro group and tyrosine-24 residue (Figure generated with PyMol (Schrodinger)).

a bystander effect (diffusion of active metabolites from the cell of origin [10]). One-electron reduction of the *para* nitro group on PR-104A (relative to the nitrogen mustard) by human one-electron reductases such as cytochrome P450 oxidoreductase (POR) and methionine synthase reductase (MTRR) [11,12] creates a nitro radical anion intermediate. The radical anion is back-oxidized in the presence of molecular oxygen or, in the absence of oxygen (anoxia), will undergo further electron addition to form the DNA alkylating hydroxylamine (PR-104H) or amine (PR-104M). PR-104H and PR-104M can cause inter-strand DNA crosslinks with disruption of the replication fork upon mitosis, the most likely mechanism of toxicity [13,14]. Hypoxia selectivity was demonstrated in a range of cancer cell lines, with hypoxia cytotoxicity ratios (HCR; aerobic IC_{50} value divided by anoxic IC_{50} value) ranging from 5 to 100-fold [10]. However despite clear evidence for hypoxia-selective activation, atypical aerobic sensitivity of some cell lines to PR-104A suggested the presence of an aerobic reductase. The human oxidoreductase AKR1C3 (aldo-keto reductase member 1C3; P42330) was subsequently shown to reduce PR-104A in an oxygen independent (two-electron) manner by bypassing the formation of the oxygen-sensitive nitro radical intermediate, and is now accepted as the major determinant of aerobic PR-104A sensitivity [15].

AKR1C3 is a type 2 3α-HSD (hydroxysteroid dehydrogenase) and type 5 17β-HSD/prostaglandin F synthase [16], and is expressed at high levels in CD34+ myeloid progenitor cells [17]. Expression of AKR1C3 in these cells is a likely explanation for the underlying mechanism of the myelosuppression observed in humans after treatment with high doses of PR-104. Initial Phase I studies of PR-104 in patients with solid tumors determined that the primary dose-limiting toxicity was myelosuppression, predominantly neutropenia and thrombocytopenia, with delayed onset that was sometimes prolonged or irreversible [18,19]. This toxicity restricted the plasma exposure of PR-104A in humans to approximately one-third of the levels achievable in mice; mean plasma AUC of 39 μM-h is recorded in humans at 1100 mg/m^2 [18,19], compared to 120 μM-h in mice at 2144 mg/m^2 [20]. The inability of PR-104 to achieve sufficiently high plasma exposures in humans has limited its clinical utility in solid tumors.

Nevertheless the improved potency and bystander effect of PR-104A relative to CB1954 make it a potential candidate for GDEPT. PR-104A demonstrated a 9-fold improvement in anti-proliferative activity when compared to CB1954 in NfsB-expressing cells [21], and there is strong evidence for larger bystander effects from the dinitrobenzamide mustard class of compounds at tissue-like cell densities [22,23]. This evidence, taken together with the large therapeutic ratio demonstrated for PR-104A *in vitro* (WT:NfsB IC_{50} ratio of 2300-fold [21]), suggests that PR-104A remains a viable candidate for nitroreductase-based GDEPT. Consistent with this rationale, PR-104 has been evaluated in pre-clinical models with considerable success [24].

Ideally a GDEPT prodrug should be an exclusive substrate for a vector-encoded enzyme. PR-104A is subject to aerobic metabolism by human AKR1C3 and hypoxic metabolism by various one-electron oxidoreductases, which may limit the therapeutic specificity of the prodrug for NTR-armed vectors. In this study we have used rational drug design to develop more selective GDEPT prodrugs. We hypothesized that elimination of the *ortho* nitro of PR-104 would reduce the ability of AKR1C3 to recognize the dinitro motif. We also predicted that, in the absence of the electron-withdrawing effect of the *ortho* nitro group, the one-electron affinity ($E(1)$) of the remaining (*para*) nitro group would be lowered below that required for metabolism by human oxidoreductase enzymes [25], while retaining capacity for two-electron reduction by bacterial NTR enzymes [26]. The use of a single nitro group as the "bioreductive switch" should also provide more reactive/cytotoxic hydroxylamine and amine metabolites than PR-104H and PR-104M, as the residual deactivating influence (electron withdrawing nature) of the *ortho* nitro group would be absent. Based on the above hypotheses, we reasoned that replacement of the *ortho* nitro group of PR-104A with hydrogen would provide a suitable prodrug for selective activation by bacterial NTR enzymes. Here we report the novel PR-104A analog SN34507, and its water-soluble 'pre-prodrug' SN35539. We also identify the major *E. coli* NTR NfsA as an effective activating enzyme of SN34507 and demonstrate significantly improved therapeutic activity of this enzyme/prodrug combination over that of NfsA/PR-104 in an HCT116 colorectal cancer xenograft model.

2. Methods and materials

2.1. Chemicals

PR-104A was synthesized, purified and stored as previously reported [27,28]. PR-104 was supplied by Proacta, Inc. SN34037 was synthesized as previously reported [29].

2.2. Generation of a PR-104A binding model for AKR1C3

A three dimensional model of PR-104A was generated using the SKETCHER module followed by CONCORD(v.6.1.3) implemented within the SYBYL(v8.0.3) molecular modeling package (TRIPOS, St Louis, MO). A single low energy conformer was then generated by OMEGA(v2.2.1; OpenEye Scientific Software, Sante Fe, NM) using the MMFF94s forcefield, with the dielectric set at 80, the maximum number of conformers generated set to 30,000 and RMS set at 1. The low energy PR-104A conformer was then docked into the active site of the AKR1C3 enzyme with flufenamic acid

Please cite this article in press as: A.M. Mowday et al., Rational design of an AKR1C3-resistant analog of PR-104 for enzyme-prodrug therapy, Biochem. Pharmacol. (2016), http://dx.doi.org/10.1016/j.bcp.2016.07.015

bound (PDB code 1S2C) using GOLD(v4.1.2) [30]. The AKR1C3 flufenamic acid structure was prepared for molecular docking by removing all water atoms and adding hydrogen atoms using SYBYLv8.0.3. Molecular docking was performed using the Goldscore fitness function. The docking site was defined as a 20 Å cavity centered on the carbon atom of the hydride transfer site in the nicotinamide ring of the NADP co-factor. The search efficiency was set at 200% and 20 Genetic Algorithm runs were performed with all poses kept. Both protein and ligand atom types were automatically defined, the option to use a ring template was enabled, and pyramidal nitrogen atoms and amide bonds were allowed to flip. The soft potentials 1 option was applied to phenylalanine 306, tryptophan-227 and phenylalanine-311. Only poses that predicted an interaction with the oxyanion hole were considered further.

2.3. Synthesis of SN34507 and SN35539

The prodrug SN34507 was prepared from commercially available 2-fluoro-5-nitrobenzoic acid in 5 steps. A further 2 steps provided phosphate pre-prodrug SN35539.

2.3.1. 2-Fluoro-5-nitro-N-(2-((tetrahydro-2H-pyran-2-yl)oxy)ethyl) benzamide (**2**)

A stirred solution of 2-fluoro-5-nitrobenzoic acid **1** (Matrix Scientific, USA) (4.56 g, 24.63 mmol) in $SOCl_2$ (Scharlau Chemicals, Spain) (50 mL) and DMF (Acros Organics, USA) (3 drops) was heated under reflux for 4 h. Excess $SOCl_2$ was removed by distillation under reduced pressure and the residue was dissolved in THF (Acros Organics, USA) (30 mL), cooled to −10 °C and treated with 2-((tetrahydro-2*H*-pyran-2-yl)oxy)ethanamine (Sigma Aldrich, Germany) (3.93 g, 27.10 mmol) then warmed to room temperature for 30 min. The solvent was evaporated and the residue dissolved in EtOAc (Macron Fine Chemicals, USA), washed with water (3×) and brine, dried with Na_2SO_4 (Scharlau Chemicals, Spain) and concentrated under reduced pressure. The crude product was purified by chromatography on silica eluting with EtOAc/Hexane (1:1) (Macron Fine Chemicals, USA) to give the amide **2** (3.17 g, 41%) as a colorless oil. ^{1}H NMR [$(CD_3)_2SO$] δ 8.67 (br, 1H), 8.42–8.38 (m, 2H), 7.64–7.59 (m, 1H), 4.62 (t, J = 3.5 Hz, 1H), 3.55–3.41 (m, 5H), 1.79–1.70 (m, 1H), 1.66–1.60 (m, 1H), 1.53–1.41 (m, 5H). HRMS(ESI) calcd for $C_{14}H_{17}FN_2NaO_5$ $[M+Na]^+$ m/z 335.1014: found 335.1014.

2.3.2. 2-(Bis(2-hydroxyethyl)amino)-5-nitro-N-(2-((tetrahydro-2H-pyran-2-yl)oxy)ethyl) benzamide (**3**)

Amide **2** (3.17 g, 10.15 mmol) was dissolved in dioxane (Acros Organics, USA) (150 mL) and treated with Et_3N (J.T.Baker Chemicals, The Netherlands) (4.24 mL, 30.45 mmol) and diethanolamine (Sigma Aldrich, Germany) (3.89 mL, 40.60 mmol). The reaction mixture was heated to 55 °C overnight then cooled to room temperature, and the solvent was evaporated. The residue was dissolved in EtOAc, washed with water (3×) and brine, dried with Na_2SO_4 and concentrated under reduced pressure. The crude product was purified by chromatography on silica eluting with EtOAc/Hexane (3:1) to give diol **3** (3.51 g, 87%) as a yellow gum. ^{1}H NMR [$(CD_3)_2SO$] δ 8.71 (t, J = 5.5 Hz, 1H), 8.10–8.06 (m, 2H), 7.17 (d, J = 9.0 Hz, 1H), 4.73 (t, J = 5.3 Hz, 2H), 4.62–4.60 (m, 1H), 3.80–3.72 (m, 2H), 3.57–3.49 (m, 5H), 3.47–3.40 (m, 7H), 1.77–1.70 (m, 1H), 1.66–1.61 (m, 1H), 1.50–1.46 (m, 4H).

2.3.3. ((4-Nitro-2-((2-((tetrahydro-2H-pyran-2-yl)oxy)ethyl)carbamoyl) phenyl)azanediyl)bis(ethane-2,1-diyl) dimethanesulfonate (**4**)

A solution of diol **3** (6.01 g, 15.12 mmol) in CH_2Cl_2 (180 mL) was cooled to 0 °C and treated with Et_3N (7.38 mL, 52.93 mmol) followed by methanesulfonyl chloride (Acros Organics, USA) (4.40 mL, 45.36 mmol). The reaction mixture was warm to room temperature for 30 min, then washed with water (3×), dried with Na_2SO_4 and concentrated under reduced pressure. The residue was purified by chromatography on silica eluting with CH_2Cl_2/MeOH (20:1) (Macron Fine Chemicals, USA) to give bis-mesylate **4** (8.04 g, 96%) as a yellow gum. ^{1}H NMR [$(CD_3)_2SO$] δ 8.73 (t, J = 5.5 Hz, 1H), 8.15–8.10 (m, 2H), 7.27 (d, J = 9.2 Hz, 1H), 4.32 (t, J = 5.3 Hz, 4H), 3.82–3.74 (m, 6H), 3.56–3.40 (m, 5H), 3.13 (s, 6H), 1.76–1.71 (m, 1H), 1.68–1.61 (m, 1H), 1.50–1.47 (m, 4H).

2.3.4. ((2-((2-Hydroxyethyl)carbamoyl)-4-nitrophenyl)azanediyl)bis (ethane-2,1-diyl) dimethanesulfonate (**5**)

A solution of bis-mesylate **4** (3.03 g, 5.47 mmol) in dry MeOH (Macron Fine Chemicals, USA) (100 mL) was treated with methanesulfonic acid (Sigma Aldrich, Germany) (17.8 mL, 20.37 mmol). The reaction mixture was stirred at room temperature for 20 min and the solvent was evaporated. The residue was dissolved in EtOAc, washed with water (3×), dried with Na_2SO_4 and concentrated under reduced pressure. The crude product was purified by chromatography on silica eluting with CH_2Cl_2/MeOH (19:1) to give alcohol **5** (1.92 g, 75%) as a yellow gum. ^{1}H NMR [$(CD_3)_2SO$] δ 8.73 (t, J = 5.5 Hz, 1H), 8.15–8.10 (m, 2H), 7.27 (d, J = 9.2 Hz, 1H), 4.32 (t, J = 5.3 Hz, 4H), 3.82–3.74 (m, 6H), 3.56–3.40 (m, 5H), 3.13 (s, 6H), 1.76–1.71 (m, 1H), 1.68–1.61 (m, 1H), 1.50–1.47 (m, 4H). HRMS(ESI) calcd for $C_{15}H_{23}N_3NaO_{10}S_2$ $[M+Na]^+$ m/z 492.0717: found 492.0720.

2.3.5. 2-((2-Bromoethyl)(2-((2-hydroxyethyl)carbamoyl)-4-nitrophenyl)amino)ethyl methanesulfonate (SN34507)

To a solution of alcohol **5** (8.00 g, 17.04 mmol) in acetone (240 mL) was added LiBr (Sigma Aldrich, Germany) (1.48 g, 17.04 mmol). The reaction mixture was stirred overnight at room temperature before the solvent was removed. The residue was dissolved in EtOAc, washed with water (2×), dried with Na_2SO_4 and concentrated under reduced pressure. The crude product was purified by flash column chromatography on silica gel eluting with CH_2Cl_2/MeOH (20:1) to give SN34507 (3.74 g, 48%) as a yellow gum. ^{1}H NMR [$(CD_3)_2SO$] δ 8.65 (t, J = 5.6 Hz, 1H), 8.14–8.09 (m, 2H), 7.22 (d, J = 9.1 Hz, 1H), 4.75 (br, 1H), 4.31 (t, J = 5.4 Hz, 2H), 3.80–3.74 (m, 5H), 3.65–3.53 (m, 5H), 3.13 (s, 3H). HRMS(ESI) calcd for $C_{14}H_{21}BrN_3O_7S$ $[M+H]^+$ m/z 454.0278: found 454.0273.

2.3.6. 2-((2-Bromoethyl)(2-((2-((di-tert-butoxyphosphoryl)oxy) ethyl)carbamoyl)-4-nitrophenyl)amino)ethyl methanesulfonate (**6**)

To a stirred solution of SN34507 (2.61 g, 5.76 mmol) in DMF (2 mL) at 10 °C, was added 1*H*-tetrazole (Sigma Aldrich, Germany) (61.9 mL, 26.50 mmol; 3% w/w solution in MeCN), followed by di-*tert*-butyl diisopropylphosphoramidite (Chem-Impex International, USA) (95%, 7.68 mL, 23.05 mmol) dropwise. The mixture was stirred at room temperature for 4 h, then cooled to 5 °C and treated with *m*-CPBA (Sigma Aldrich, Germany) (70%, 7.46 g, 43.21 mmol) portion wise, before being warmed to room temperature for 2 h. The reaction was then concentrated and the residue dissolved in EtOAc, washed with 10% aqueous $Na_2S_2O_5$ (Scharlau Chemicals, Spain), 5% aqueous $NaHCO_3$ (Scharlau Chemicals, Spain) and water before being dried with Na_2SO_4 and concentrated *in vacuo*. The crude product was purified by chromatography on silica eluting with EtOAc/Hexane (1:1) to give phosphate ester **6** (1.45 g, 39%) as a yellow gum. ^{1}H NMR [$(CD_3)_2SO$] δ 8.84 (t, J = 5.6 Hz, 1H), 8.13 (2d, J = 2.8 Hz, 1H), 8.09 (d, J = 2.8 Hz, 1H), 7.23 (d, J = 9.3 Hz, 1H), 4.32 (t, J = 5.4 Hz, 2H), 4.00 (q, J = 6.3 Hz, 2H), 3.80–3.74 (m, 4H), 3.64 (t, J = 6.7 Hz, 2H), 3.51 (q, J = 5.6 Hz, 2H), 3.14 (s, 3H), 1.42 (s, 18H). HRMS(ESI) calcd for $C_{22}H_{37}BrKN_3O_{10}PS$ $[M+K]^+$ m/z 684.0752: found 684.0740.

Please cite this article in press as: A.M. Mowday et al., Rational design of an AKR1C3-resistant analog of PR-104 for enzyme-prodrug therapy, Biochem. Pharmacol. (2016), http://dx.doi.org/10.1016/j.bcp.2016.07.015

2.3.7. 2-((2-Bromoethyl)(4-nitro-2-((2-(phosphonooxy) ethyl)carbamoyl)phenyl)amino)ethyl methanesulfonate (SN35539)

A stirred solution of phosphate ester **6** (1.45 g, 2.24 mmol) in CH_2Cl_2 (30 mL) was treated with TFA (10 mL) at room temperature with stirring for 1 h, then concentrated under reduced pressure to remove excess TFA. The resulted yellow residue was dissolved in EtOAc and evaporated to dryness to give SN35539 (1.20 g, 100%) as a yellow gum. ^{1}H NMR [$(CD_3)_2SO$] δ 8.86 (t, J = 5.6 Hz, 1H), 8.15–8.11 (m, 2H), 7.24 (d, J = 9 Hz, 1H), 4.32 (t, J = 5.4 Hz, 2H), 4.07–4.02 (m, 2H), 3.79-3.74 (m, 4H), 3.65 (t, J = 6.7 Hz, 2H), 3.51 (q, J = 5.5 Hz, 2H), 3.13 (s, 3H). HRMS(ESI) calcd for $C_{14}H_{21}BrKN_3O_{10}PS$ $[M+K]^+$ m/z 571.9500: found 571.9451.

2.4. Preparation and storage of stock solutions

For *in vitro* studies, prodrug stocks and AKR1C3 inhibitor (SN34037) were dissolved in DMSO (Acros Organics, USA) (0.1 M) and stored at −80 °C. For *in vivo* studies, PR-104 (as sodium salt lyophilized with mannitol) (Proacta Inc, USA) was reconstituted in 2 mL water and diluted in PBS. SN35539 free acid was dissolved in phosphate-buffered saline containing two equivalents of $NaHCO_3$. Dosing solutions were prepared fresh, held at room temperature in amber vials, and used within three hours. cLogP values of the prodrugs were calculated using ChemBioDraw Ultra Version 13.0.

2.5. Cell lines and candidate gene expression

HCT116 WT cells were purchased from the ATCC (Manassas, VA, USA). HCT116 cell lines over-expressing AKR1C3 [15], POR [12] and *E. coli* NfsA [21] had been previously generated and validated for candidate gene expression as described. Frozen stocks were confirmed to be mycoplasma free by PCR enzyme-linked immunosorbent assay (ELISA) (Roche Diagnostics Corp, Basel, Switzerland). Neoplastic cell lines were cultured in α-minimal essential medium using a humidified incubator (37 °C, 5% CO_2) as previously described [10,23] for a maximum of 12 weeks. Harvested cells were counted using an electronic particle counter (Z2 Coulter Particle Analyzer, Beckman Coulter, Florida, USA).

2.6. Measurement of one-electron reduction potential

The $E(1)$ value of SN34507 was determined by measuring the fast formation of the redox equilibrium (⩽50 μs) between it and methyl viologen (Acros Organics, USA) as the redox indicator ($E(1) = -447 \pm 7$ mV), following pulse radiolysis (2.5 Gy in 200 ns) of deaerated solutions containing *tert*-butanol (0.2 M) and phosphate buffer (2.5 mM, pH 7).

2.7. Anti-proliferative (IC_{50}) assay

The anti-proliferative IC_{50} was determined as the concentration of prodrug required for 50% inhibition of cell growth, following a four hour drug exposure and five days regrowth in the absence of drug. Assays were performed under oxic or anoxic conditions as described previously [10,31], the latter using a 5% H_2/palladium catalyst scrubbed Bactron anaerobic chamber (Sheldon Manufacturing, OR, USA) to achieve severe anoxia (<10 ppm O_2 gas phase) during prodrug exposure. Total exposure of cells to anoxia did not exceed 6 h.

2.8. 3D multicellular bystander assay

Multicellular layers (MCLs) were grown and bystander effect assays were performed as previously reported [23]. The drug concentration required for 10% survival relative to untreated controls (C_{10}) was calculated by interpolation. Bystander effect efficiency (BEE) was calculated using the previously reported equation; $[\log C_{10}(T) - \log C_{10}(T_A)/\log C_{10}(T) - \log C_{10}(A)]$, where $C_{10}(T)$ is the C_{10} for target cells in MCLs grown from targets alone, $C_{10}(T_A)$ is the C_{10} for targets grown in co-culture with activators and the $C_{10}(A)$ is the C_{10} for activators in the co-cultures [32].

2.9. Statistical analysis 3D

All cell viability data were tested for significance by unpaired Student's *t*-test following confirmation each of the two samples being compared followed a normal distribution (Shapiro-Wilk normality test) (SigmaStat version 4.0 integrated with SigmaPlot version 12; Systat software, CA, USA). Significance of tumor growth delay (time for untreated control *versus* treated tumor population to exceed four-times intial treatment volume; RTV4) was evaluated by Log rank P-test (SigmaStat version 4.0 integrated with SigmaPlot version 12; Systat software, CA, USA).

2.10. Animal husbandry

Specific pathogen-free homozygous NIH-III (NIH-Lyst^{bg} Foxn1^{nu} Btk^{xid}) nude mice were obtained from Charles River Laboratories (Wilmington, MA, USA), bred in the Vernon Jansen Unit (University of Auckland), and supplied at 7–9 weeks of age. Mice were housed in groups of ⩽6 in Techniplast microisolator cages with a 12 h light/dark cycle, and were fed a standard rodent diet (Harlan Teklad diet 2018i) and water ad libitum. All animals were uniquely identifiable by ear tag number and weighed 18–25 g at the time of the experiment. All animal protocols were approved by the University of Auckland Animal Ethics Committee.

2.11. Tumor growth delay

The maximum tolerated dose of SN35539 was determined using a fixed 8-step logarithmic scale with 1.33-fold dose increments as required. A conservative starting dose was determined from related compounds. Animals were promptly culled if body weight loss exceeded 20% or if there were clinical signs of severe morbidity. The MTD was defined as the highest dose at which all animals survived with no unacceptable morbidity and mean body weight loss did not exceed 15%.

Tumors were inoculated onto the flanks of female NIH-III nude mice by subcutaneous injection of 10^7 cells. Tumor-bearing mice were randomized to treatment groups when tumors reached treatment size (300–350 mm^3) and injected with a single intraperitoneal dose of prodrug or vehicle. Tumor size and body weights were measured 2–3 per week. Tumor volume was calculated as $\pi (Lxw^2)/6$ where L is the major axis and w is the perpendicular minor axis. Animals were culled when the tumor volume had increased four-fold relative to pre-treatment volume (RTV4, survival endpoint) or if body weight loss exceeded 20% of the pre-treatment value. Kaplan Meier plots were constructed to calculate median time to endpoint. Treatment efficacy was assessed by comparing the median survival time with untreated animals using the Log-rank test P-test (SigmaStat version 4.0 integrated with SigmaPlot version 12; Systat software, CA, USA).

2.12. Core NTR over-expression library

The 58-membered candidate NTR gene over-expression library in *E. coli* strain SOS-R2 was as described in [21], with the addition of 11 additional NTR candidates. The additional NTRs included eight NfsA homologs from *Bacillus coagulans* (ATCC 7050), *Bacillus thuringiensis serovar konkukian* (str. 97-27), *Erwinia carotovora* subsp. *atrosepticum* (SCRI1043), *Lactobacillus sakei* subsp. *sakei*

(23K), *Listeria welshimeri* (ATCC 35897), *Mycobacterium smegmatis* (str. MC2 155), *Nostoc punctiforme* (PCC 73102), and Frp cloned from a different *Vibrio harveyi* (KCTC 2720) strain than that previously published (and herein referred to as Frp2_Vh). The remaining additional NTRs were KefF and YcaK from *E. coli* W3110, previously published in [33], and a previously unpublished YcaK homolog from *Pseudomonas aeruginosa* PAO1. Gene specific primers for all previously unpublished NTR candidates are listed in Table 1.

2.13. Bacterial SOS and IC_{50} assays

Screening of the NTR library for enzymes able to reduce SN34507 was carried out in *E. coli* strain SOS-R2 as previously described in full [21]. SOS-R2 is a specialized *E. coli* screening strain that contains gene knockouts of the NTRs *nfsA, nfsB, nemA, azoR* and the export pump *tolC*. It contains a genomic copy of the *lacZ* reporter gene under control of a SOS promoter *sfiA* meaning the DNA damage experienced by this reporter strain leads to a quantifiable increase in β-galactosidase expression. The SOS assay was carried out as previously described [21]. Briefly, in microtiter plate format NTR over-expression was induced and exponential growth phase bacteria were exposed to 10 μM of SN34507 for 4 h. Following this an aliquot of cell culture was incubated with reaction buffer containing *ortho* nitrophenyl-β-galactosidase to measure β-galactosidase levels and thus infer the DNA damage present in each individual NTR over-expression strain as a consequence of reduction of SN34507 to its DNA damaging metabolites.

For the bacterial IC_{50} assays, overnight cultures of SOS-R2 were inoculated from glycerol stocks into individual microtiter plate wells containing 200 μL of LB media supplemented with 100 μg mL^{-1} ampicillin and 0.4% glucose, and grown at 30 °C shaking at 200 rpm for ~16 h. The next morning 50 μL of overnight cultures was used to inoculate 1 mL of assay media (LB supplemented with 100 μg mL^{-1} ampicillin, 0.2% glucose and 50 μM IPTG) in individual 15 mL Falcon tubes. These were incubated at 30 °C, 200 rpm for 2.5 h, after which 30 μL aliquots of culture were added to individual wells of a 384 well microplate, each containing 30 μL of assay media supplemented with SN34507 at twice the desired final concentration (spanning 0–1000 μM in a serial dilution). In each independent experiment cultures were assayed in duplicate. The turbidity of the cultures (OD_{600}) was measured, the plate returned to 30 °C, 200 rpm for 4 h and then the OD_{600} was measured again. Relative increases in OD_{600} for drug containing vs non-drug containing wells were then used to calculate percentage growth inhibition for each over-expression strain. The IC_{50} value (drug concentration at which growth inhibition was 50% that of the unchallenged control) was calculated using Graphpad Prism 6 (*GraphPad Software Inc. La Jolla, CA, USA*).

2.14. Enzyme kinetics

Recombinant His6-tagged NTRs were purified by nickel-affinity chromatography (Novagen, Merck, Darmstadt, Germany). FMN cofactors were reconstituted and proteins were desalted, quantified, assessed for purity and stored as previously described [21]. The extinction co-efficient of SN34507 at 400 nm (ε = 13,400 M^{-1} cm^{-1}) was measured as previously described for PR-104A and steady-state enzyme kinetics for purified NTRs were assessed as previously described [21] over a SN34507 concentration range of 5–1000 μM.

2.15. Cell cycle analysis

WT and NfsA-expressing HCT116 cells were exposed to 0.05 μM of prodrug for four hours before washing and recovery in drug free media for 24 h. Cells were then fixed in ice cold pure methanol for 30 min at −20 °C and stained with propidium iodide solution (20 μg/mL) containing RNAse (100 μg/mL). Analysis of cells was performed on a flow cytometer (Becton Dickinson FACscan flow cytometer) and curves were fitted using ModFit LT software (Verity Software House).

Table 1
Primers for amplification and cloning of previously unpublished NTR candidate genes.

Primer	Sequence (5′ → 3′)
Nitroreductase specific primer for amplification and cloning into pUCX and pET28a+	
NfsA_Eca_Fw	GGGGCATATGATACCAACTATTGATTTGCTACA
NfsA_Eca_Rv	GGGGCTCGAGCTAGCGTATCGCCCATCCTTGTTG
NfsA_Bc_Fw	GGGGCATATGAATACTATCATTGAAACGATTCTC
NfsA_Bc_Rv	GGGGGTCGACTTACTTTTTATCAAACCCTTGCGT
NfsA_Np_Fw	GGCATATGCCTTTACAGATGGAA
NfsA_Np_Rv	GGGTCGACTTACAGTAGCTTGAA
NfsA_Bt_Fw	GGGGCATATGAATGAAATGATACATAAAATGGAG
NfsA_Bt_Rv	GGGGGTCGACTCATTTCTTATTTAATCCTCTCTCAT
NfsA_Ls_Fw	GGGGCATATGTCTGATTTAATCGCACAAATGCAAC
NfsA_Ls_Rv	GGGGGTCGACTTATGCTAATGTAAACCCCTGTTTCTT
NfsA_Ms_Fw	GGGGCATATGACGGTCATCGCGCGCTACGCAGACGTCGAT
NfsA_Ms_Rv	GGGGCTCGAGTCAGCGGATTCCCAGGCCCAACCGCTCG
NfsA_Lw_Fw	GGGGCATATGAATCAGGCGATAGATGCCATTTT
NfsA_Lw_Rv	GGGGGTCGACTTATTTTTGATTTAAATGTTGC
Frp2_Vh_Fw	GGGCATATGAACAATACGATTGAAA
Frp2_Vh_Rv	GGGGTCGACTTAGCGTTTTGCTAGCC
Ycak_Pa_Fw	GGGGCATATGGTTGAAACCGCCAAGACC
Ycak_Pa_Rv	GGGGGTCGACCTAGACCTGGCTGCCGAGCT

Underlined text indicates restriction sites.

3. Results

3.1. Drug design rationale for SN34507

Using the X-ray crystallographic data for AKR1C3 with flufenamic acid bound [34], potential binding modes for PR-104A were predicted by molecular docking studies, and some located the *para*-nitro group of PR-104A in the oxyanion hole within 3 Å of the bound NADP cofactor, consistent with the potential for tyrosine-55 mediated hydride transfer and observation of exclusive reduction of the *para*-nitro by recombinant AKR1C3 [15]. The ancillary *ortho* nitro group of PR-104A was directed toward the side chain hydroxyl of tyrosine-24, consistent with the absence of nitroreduction at this site by AKR1C3 (Fig. 1B). In our preferred binding mode, the mustard arms are predicted to pack against the indole side chain of tryptophan-227, while the carboxamide arm binds in part of the main active site pocket termed subpocket 1 adjacent to phenylalanine-311.

The potential for an interaction between the ancillary *ortho* nitro and tyrosine-24 prompted us to hypothesize that its elimination on the PR-104A scaffold might minimize contacts within the active site, and reduce the ability of AKR1C3 to recognize the PR-104A dinitro motif. The novel GDEPT prodrug SN34507 was thus created by substituting the *ortho* nitro group of PR-104 with hydrogen (Fig. 1A). Simplifying the PR-104A prodrug scaffold to a single *para*-nitro group was also hypothesized to lower the one-electron affinity ($E(1)$) of the remaining (*para*) nitro group below that required for metabolism by human oxidoreductase enzymes such as POR, as well as providing more reactive/cytotoxic hydroxylamine and amine metabolites. We synthesized SN34507 (and its corresponding phosphate ester pre-prodrug SN35539) as described (Fig. 2).

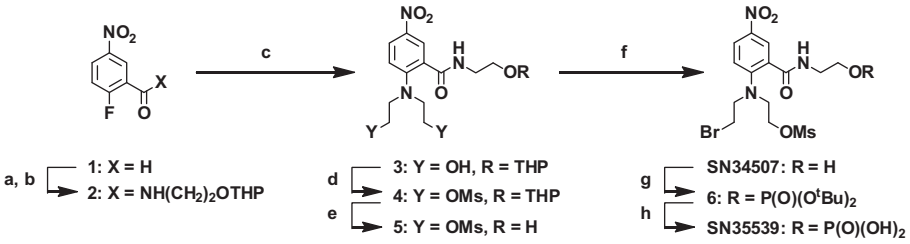

a) $SOCl_2$, DMF, 80 °C; b) $H_2N(CH_2)_2OTHP$, THF, -10 °C to RT; c) diethanolamine, dioxane, Et_3N, 55 °C; d) MsCl, Et_3N, DCM, 0 °C; e) MsOH, MeOH; f) 1 eq LiBr, acetone; g) di-*tert*-butyl-*N,N*-diisopropylphosphoramidite, 1*H*-tetrazole, DMF, 5 °C to RT then *m*-CPBA, 0 °C; h) TFA, DCM, 5 °C to RT

Fig. 2. The synthesis of SN34507 and SN35539.

3.2. SN34507 is not a biologically relevant substrate for human AKR1C3

To test whether SN34507 was cytotoxic in the presence of human AKR1C3, the sensitivity of HCT116 WT cells (WT cells) and HCT116 cells overexpressing AKR1C3 (AKR1C3 cells) to SN34507 or PR-104A was examined under aerobic conditions using a low cell density anti-proliferative IC_{50} assay. The WT IC_{50} values for SN34507 and PR-104A were comparable, being 111 ± 6 μM and 70 ± 11 μM respectively. AKR1C3 over-expression in this cell line increased the anti-proliferative effect of PR-104A by 87.3-fold, but had minimal effect on SN34507 (2.9-fold). To confirm elevation in AKR1C3 catalytic activity was responsible for cellular hypersensitivity to PR-104A, pharmacological inhibition of AKR1C3 was achieved with the morpholylurea SN34037 [29]. This provided essentially complete cytoprotection of AKR1C3 cells from PR-104A exposure, suppressing the observed 87-fold sensitization effect (WT:AKR1C3 IC_{50} ratio) to 1.7-fold (Fig. 3a). In contrast, the effect of AKR1C3 inhibition on SN34507 treated cells was minor (2.9-fold sensitivity modified to 1.3-fold, Fig. 3a), although this difference achieved significance ($P = 0.023$, Student's *t*-test) suggesting the possibility of trace activation. The AKR1C3 inhibitor itself had no demonstrable anti-proliferative effect on WT cells (data not shown). Other AKR1C family members (AKR1C1, AKR1C2, and AKR1C4) were unable to sensitize cells to PR-104A or SN34507 under these conditions (Fig. 3b).

A limitation of low cell density anti-proliferative assays is that a portion of intracellular cytotoxic drug metabolites may be lost into the extracellular media through passive diffusion and thereby confound the absolute IC_{50} value. Therefore multi-cellular layer (MCL) culture models were employed to investigate cytotoxic potency at tissue-like cell densities, ensuring all local metabolite redistribution contributes to the overall pharmacodynamic endpoint (loss of clonogenic viability). After prodrug exposure (10 μM), 100% WT MCLs demonstrated similar cell plating efficiencies (0.82 and 0.70 for PR-104A and SN34507 respectively, $P = 0.12$, Student's *t*-test). In 100% AKR1C3 MCLs, treatment with 10 μM PR-104A produced a $>10^4$-fold decrease (4.06 log cell kill) in plating efficiency, in contrast to SN34507 treatment which produced a 1.1-fold decrease in plating efficiency (Fig. 3c). Notably, the plating efficiencies for 100% WT and 100% AKR1C3 MCLs treated with SN34507 were not significantly different ($P = 0.90$, Student's *t*-test). Collectively, the *in vitro* data indicate that PR-104A is bioactivated by AKR1C3 under aerobic conditions while the prodrug analog SN34507 is essentially free of this activity.

To test whether AKR1C3 metabolism *in vivo* was biologically relevant for SN34507 activity we determined the role of AKR1C3 in the anti-tumor efficacy of the phosphate 'pre-prodrugs' PR-104 or SN35539 (Fig. 1A). Each pre-prodrug was administered as a single intraperitoneal injection at the maximum tolerated dose of 1330 μmol/kg in a growth delay assay using subcutaneous HCT116 tumor xenografts engineered to over-express AKR1C3. Tumors treated with SN35539 grew at a similar rate to the vehicle treated (control) tumors, while significant tumor control was observed following PR-104 treatment (Fig. 3d). The median time to endpoint (four times the original treatment volume, RTV4) for the control and SN35539 treated groups was 12 days ($P = 0.70$, Log-rank test). A significant increase to 44 days was observed in the PR-104 treated group ($P = 0.001$ compared to untreated tumors, Log-rank test). The *in vivo* data further support the conclusion that AKR1C3 does not play a biologically relevant role in sensitivity to the prodrug SN34507.

3.3. SN34507 is not significantly activated under anoxic conditions

The one-electron reduction potential of SN34507 was determined by pulse radiolysis. Observations at 600 nm for 3 mixtures of compound and indicator, gave $K = 0.16 \pm 0.05$ which, on applying the Nernst equation and allowing for ionic strength effects, yielded the value $E(1) = -503 \pm 10$ mV for SN34507. To determine whether anoxic metabolism had been minimized, HCT116 WT cells or POR over-expressing HCT116 cells (POR cells) were exposed to SN34507 under anoxic or aerobic conditions. Anti-proliferative IC_{50} assays were used to calculate hypoxia cytotoxicity ratios. The HCR for PR-104A increased significantly from 18-fold in WT cells to 126-fold in POR cells ($P = 0.048$, Student's *t*-test), as expected. In contrast there was minimal anoxic selectivity for SN34507 in either WT or POR cells (1.2-fold and 2.4-fold respectively, $P = 0.12$, Student's *t*-test), indicating that SN34507 lacks significant anoxia-selective anti-proliferative activity and is a poor single-electron acceptor (Fig. 4). Collectively these data indicate the low electron affinity of SN34507 eliminates the majority of reduction by human one-electron reductases such as POR.

3.4. Use of a bacterial screen to identify nitroreductase enzymes that activate SN34507

After confirming that SN34507 was not a significant substrate for the major one- and two-electron reductases POR and AKR1C3, we next sought to identify a suitable exogenous two-electron (type I) nitroreductase to bioactivate SN34507. A multi-family bacterial oxidoreductase gene library [21], including several novel candidates (Table 1) was challenged with SN34507, and the level of SOS induction for each NTR was measured (Fig. 5).

The seven *E. coli* NTR strains that induced the greatest SOS response to SN34507 (i.e., those expressing *Salmonella typhi* NfsA, *E. coli* NfsA, *Citrobacter koseri* NfsA, *Listeria welshmerii* NfsA, *Enterobacter sakazakii* NfsA, *Vibrio harveyi* Frp and *Vibrio fischeri* FRase) were taken forward into anti-proliferative bacterial IC_{50} assays to confirm that levels of SOS induction were predictive of cytotoxic

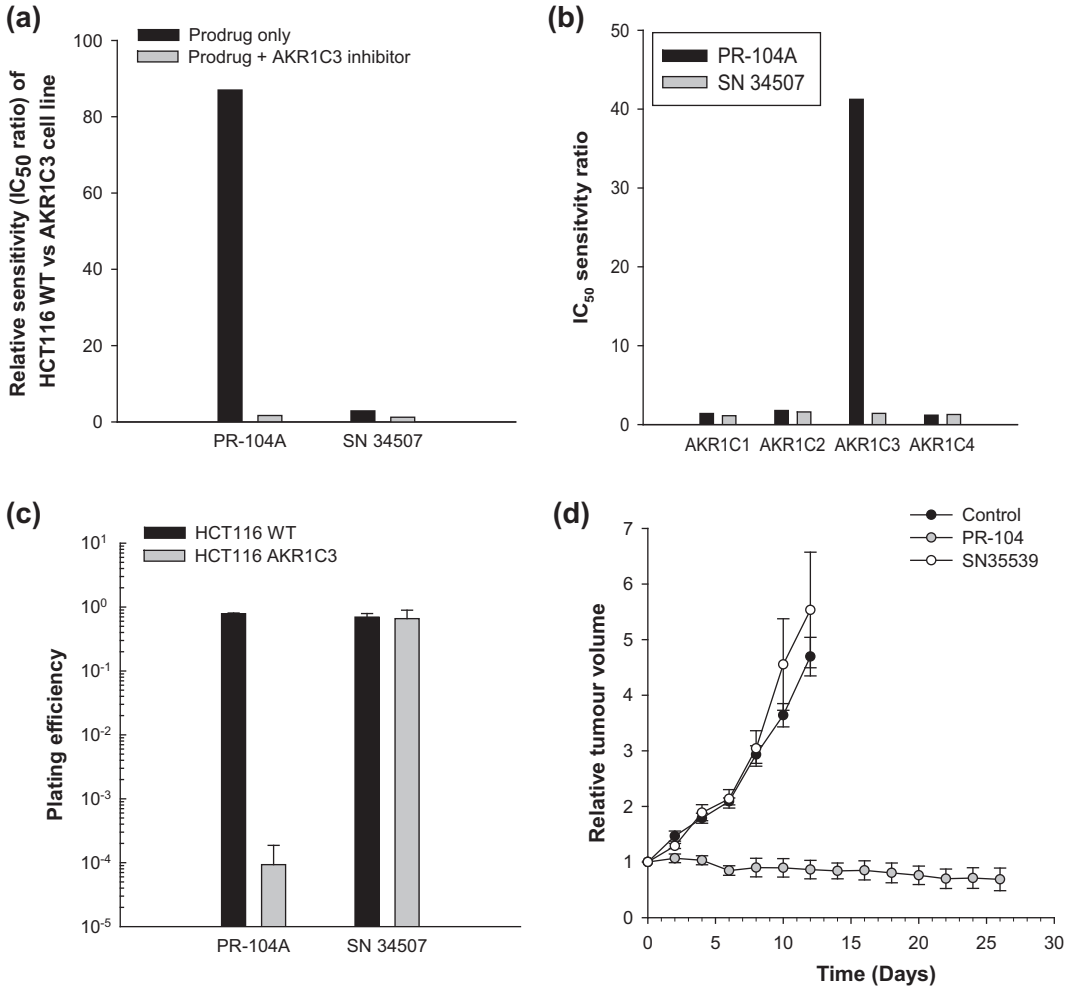

Fig. 3. The prodrug SN34507 is not a substrate for human aldo-keto reductase 1C3: (a) Relative sensitivity (interexperimental IC_{50} ratio at low cell density for ⩾3 independent experiments) of HCT116 WT and its AKR1C3 expressing isogenic cell line to prodrugs PR-104A or SN34507 in the presence or absence of the selective AKR1C3 inhibitor SN34037; (b) Additional AKR1C family members AKR1C1, AKR1C2, and AKR1C4 were unable to sensitize cells to PR-104A or SN34507 under these conditions (mean of ⩾3 independent experiments); (c) Average plating efficiency from 3 independent experiments of HCT116 WT and its AKR1C3 expressing isogenic cell line following exposure to prodrugs PR-104A or SN34507 (10 μM) at tissue-like cell density; (d) Relative growth inhibition of HCT116 AKR1C3-expressing tumor model in nude mice following a single administration of the AKR1C3-activated pre-prodrug PR-104 (1330 μmol/kg, ip) or the AKR1C3-resistant pre-prodrug SN35539 (1330 μmol/kg, ip). N = 6 tumors per treatment group.

potential. Four other members of the library (*E. coli* NfsB, NemA, AzoR, MdaB) were included for diversity. The calculated IC_{50} values (i.e. the concentration of SN34507 that yielded 50% turbidity relative to an unchallenged control) are presented in Table 2. NfsA family members were confirmed as the preferred bacterial NTR enzymes for SN34507, demonstrating IC_{50} values of <400 μM (range; 282–395 μM).

Based on the results of the IC_{50} screen, three NTRs were selected for expression and purification as His6-tagged recombinant proteins; *S. typhi* NfsA, *E. coli* NfsA and *C. koseri* NfsA. Apparent SN34507 kinetic parameters were calculated for each enzyme by measuring reaction rates at varying substrate concentrations and a fixed concentration of NADPH (the preferred electron donor for each enzyme) (Table 3). The k_{cat}/K_m was greatest for *E. coli* NfsA, identifying this NTR as a promising NTR candidate for SN34507 activation.

3.5. E. coli NfsA is an efficient activator of SN34507 in vitro and in vivo

The possible utility of the *E. coli* NfsA/SN34507 enzyme/prodrug combination was investigated in a human cell line model, using previously generated HCT116 cells over-expressing *E. coli* NfsA [21]. Initially, anti-proliferative potency of SN34507 was compared to PR-104A following four hour drug exposure under aerobic conditions (Fig. 6a). Both PR-104A and SN34507 prodrugs were highly active against the NfsA cell line with anti-proliferative IC_{50} values of 0.025 ± 0.004 μM and 0.065 ± 0.015 μM respectively, confirming SN34507 as a suitable prodrug substrate for *E. coli* NfsA *in vitro*.

The four and six electron reduction products of PR-104A (PR-104H and PR-104M, respectively) are known to alkylate DNA, causing cross-linking of DNA strands and preventing uncoiling of the DNA double helix [10,14]. DNA replication is subsequently arrested at the G_2/M DNA damage checkpoint, with cell death occurring when cross-links are not repaired. To test whether that the anti-proliferative effect of SN34507 was occurring via a similar mechanism of cell cycle arrest, WT and NfsA cells were exposed to equimolar concentrations (0.05 μM) of PR-104A or SN34507 before recovery and subsequent cell cycle analysis (Fig. 6b). Following treatment WT cell cycle redistribution was unchanged, with G_2/M population similar to the untreated control cells (21% and 25%, respectively). However with the NfsA cells, the percentage of cells in G_2/M increased from 14% (control) to 26% and 64% for PR-104A and SN34507 treated cells, respectively. This indicates that NfsA-mediated activation of SN34507 results in arrest of

Please cite this article in press as: A.M. Mowday et al., Rational design of an AKR1C3-resistant analog of PR-104 for enzyme-prodrug therapy, Biochem. Pharmacol. (2016), http://dx.doi.org/10.1016/j.bcp.2016.07.015

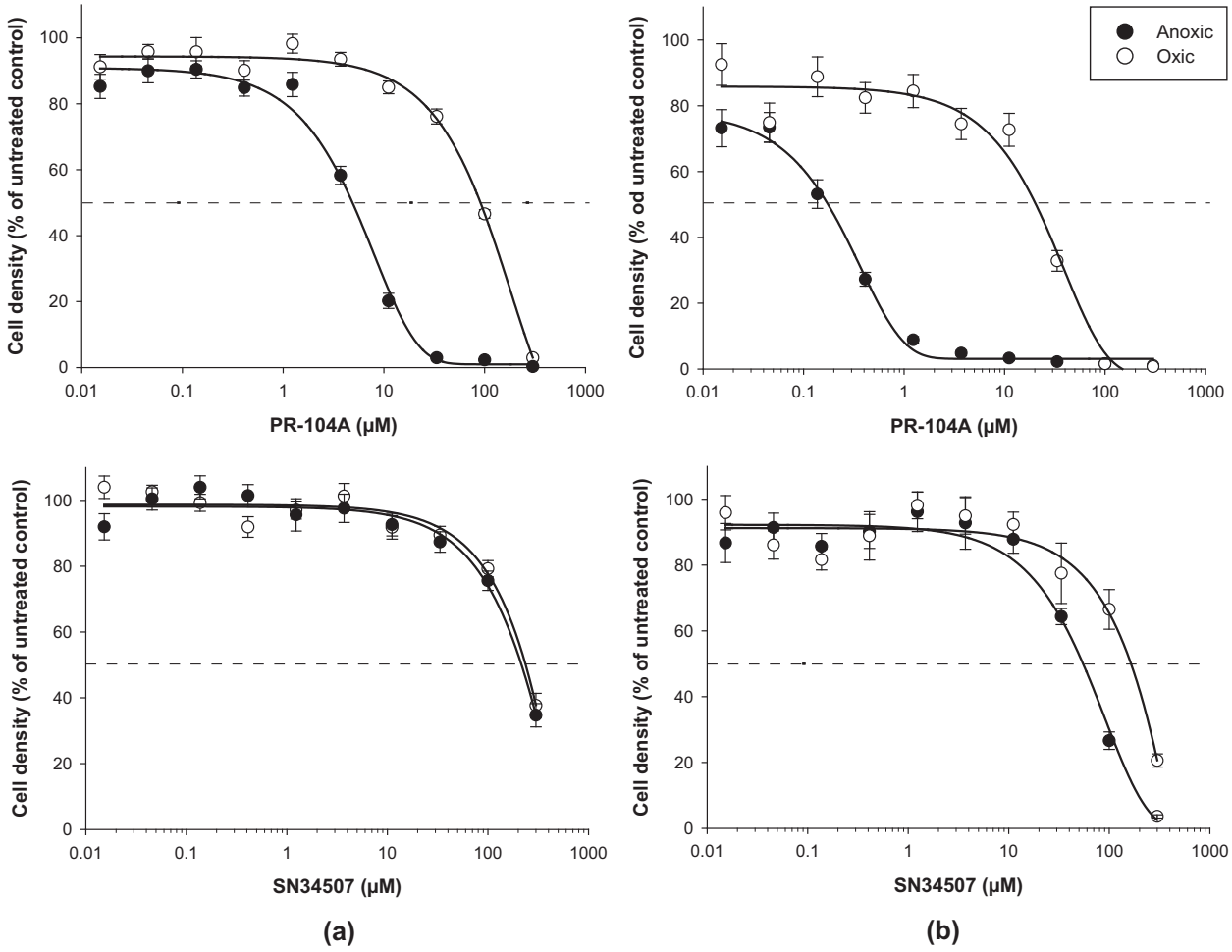

Fig. 4. The prodrug SN34507 is a poor substrate for one-electron bioactivation under anoxic conditions: (a) Dose-response curve of HCT116 WT cells exposed to PR-104AA (upper graph) or SN34507 (lower graph) under aerobic (○) or anoxic (●) conditions; (b) Dose-response curve of HCT116 isogenic POR-expressing cells exposed to PR-104A (upper graph) or SN34507 (lower graph) under aerobic (○) or anoxic (●) conditions. Data are the average of three independent experiments ± SD.

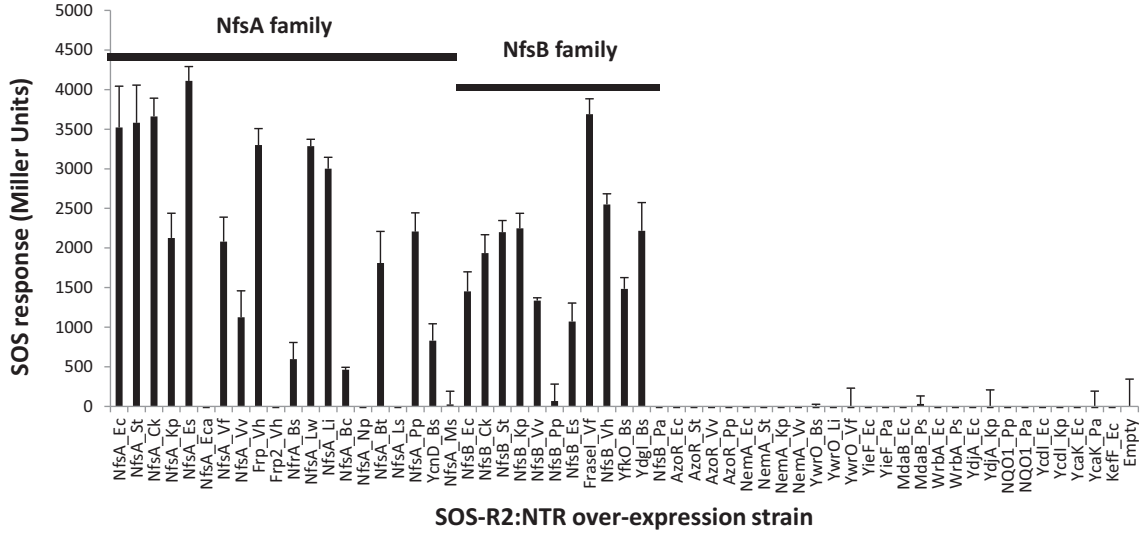

Fig. 5. Bacterial SOS response in SOS-R2:NTR strains challenged with SN34507: SOS response levels were measured following 4 h challenge with 20 μM SN34507. SOS response represents the difference in Miller Units (a measure of β-galactosidase activity) between challenged and unchallenged cultures of the same over-expression strain. Data are the average of three independent assays ± SD.

Please cite this article in press as: A.M. Mowday et al., Rational design of an AKR1C3-resistant analog of PR-104 for enzyme-prodrug therapy, Biochem. Pharmacol. (2016), http://dx.doi.org/10.1016/j.bcp.2016.07.015

Table 2
Growth inhibition of NTR-overexpressing SOS-R2 after a four hour challenge with increasing concentrations of SN34507.

Source	Family	IC50 (μM)
E. coli	NfsA	308 ± 23
S. typhi	NfsA	282 ± 16
C. koseri	NfsA	330 ± 13
L. welshmerii	NfsA	348 ± 35
E. sakazakii	NfsA	351 ± 11
V. harveyi	Frp	395 ± 35
E. coli	NfsB	474 ± 26
V. fischeri	FRase	480 ± 48
E. coli	MdaB	>1000
E. coli	Azo	>1000
E. coli	NemA	>1000
–	Empty	>1000

Table 3
Bacterial nitroreductase recombinant enzyme steady state kinetics.

NTR	K_m[a] (μM)	k_{cat}[a] (s^{-1})	k_{cat}/K_m[b]
E. coli NfsA	358 ± 44	3.0 ± 0.15	8.4
S. typhi NfsA	14 ± 2.1	0.086 ± 0.0036	6.1
C. koseri NfsA	507 ± 71	1.39 ± 0.1	2.7

[a] Apparent kinetic parameters as measured at 300 μM NADPH.
[b] (mM^{-1} s^{-1}).

DNA replication and accumulation of cells at the G_2/M DNA damage checkpoint, as previously seen for PR-104A.

To model the ability of SN34507 to penetrate tumor tissue, become metabolically activated by NfsA-expressing cells and subsequently redistribute from these 'activator' cells to sterilize neighboring NfsA negative 'target' (WT) cells, intimate mixtures of 3% HCT116 NfsA + 97% HCT116 WT cells were grown in 3D MCL models (Fig. 7a). Under these tissue-like densities SN34507 was more selective for activator cells than was PR-104A, as determined by the ratio of potencies against NTR negative targets (T) grown without activators and the activators (Ac) in co-cultures (T/Ac ratio of 464 for SN34507 *versus* 250 for PR-104A), indicating a greater therapeutic ratio for SN34507 at physiologically relevant cell densities. PR-104A was modestly more dose-potent than SN34507 against NfsA-positive activators in MCL co-cultures (Activator C_{10} values of 0.12 and 0.59 μM respectively) (Fig. 7b).

The increase in sensitivity of the target cells in the presence of 3% activator cells was greater for PR-104A than SN34507, as demonstrated by the increased left-shift of the target cell survival curves in the presence of NfsA activator cells (gray filled circles, Fig. 7). This indicates that the active metabolites of PR-104A have superior tissue diffusion properties over those of SN34507, and thus possess an enhanced bystander cell killing ability. The magnitude of this phenomenon (the bystander effect efficiency, BEE) was calculated from the C_{10} values as previously described. Under these conditions, PR-104A provided a BEE of 68%, whereas the BEE value for SN34507 was approximately half this value, 38%, under identical conditions. Prodrug partition coefficients ($LogD_{7.4}$) for PR-104A and SN34507 were calculated to be 1.0 and 0.73 respectively, indicating PR-104A and associated metabolites are more lipophilic than SN34507. Moreover the reactivity of SN34507 reduced metabolites will be greater due to the absence of the electron withdrawing *ortho* nitro. Both of these aspects are likely to contribute to the reduced bystander effect observed for SN34507 relative to PR-104A.

We have previously used mixed xenograft models expressing a minority of NTR positive cells to compare efficacy of prodrugs for gene therapy [22,35], as this necessitates the presence of a robust prodrug bystander effect (cytotoxic metabolite redistribution) to achieve an anti-tumor growth delay and mimics heterogeneous vector distribution. Using this methodology we compared the anti-tumor activity of PR-104 and SN35539 *in vivo* using xenografts grown from 100% HCT116 WT (Fig. 8a) or from mixtures containing 30% NfsA cells (Fig. 8b). Tumor-bearing mice were treated with a single IP dose of prodrug and the tumor size was monitored. SN35539 was administered at the MTD of 1330 μmol/kg and PR-104 was administered at 388 μmol/kg, the mouse equivalent dose that provides a plasma AUC_{inf} (39 μM-h) comparable to the human three-weekly (q3w) MTD of 1100 mg/m^2 [19,20].

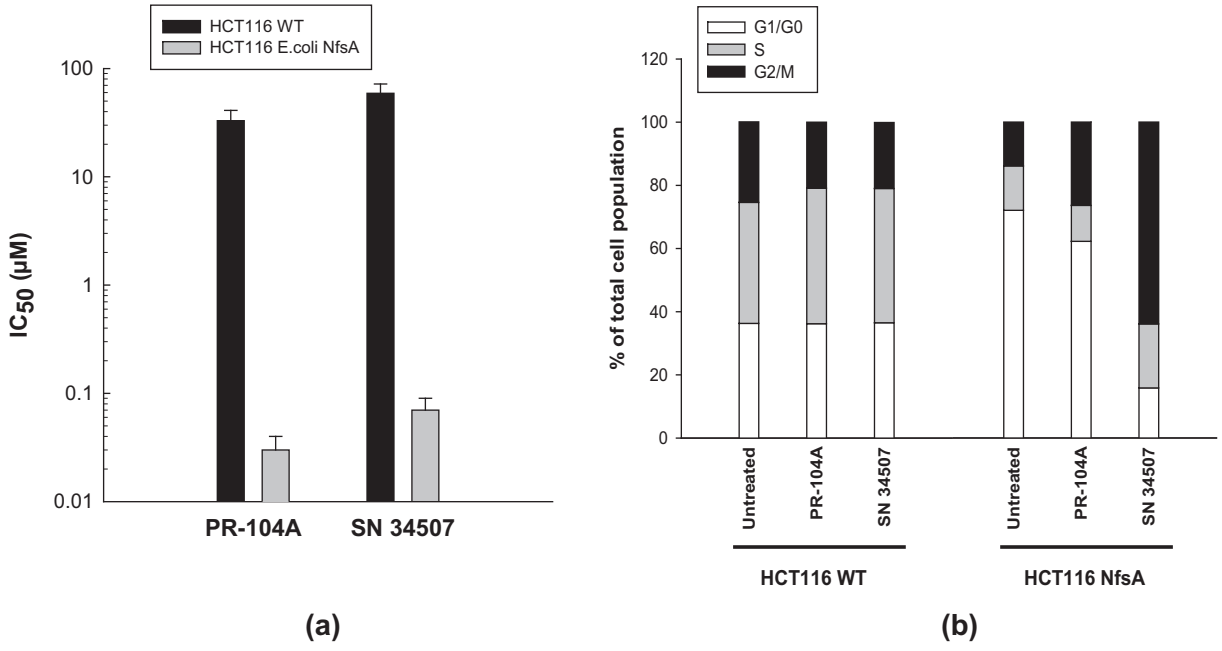

Fig. 6. *E. coli* NfsA-dependent activation of SN34507 and PR-104A in low density cell line cultures: (a) Relative anti-proliferative activity (IC_{50} value (μM), mean ± sem) of the prodrugs PR-104A and SN34507 against the HCT116 WT cell line and its *E. coli* NfsA-expressing isogenic cell line under aerobic conditions; (b) Cell cycle distribution of HCT116 WT and NfsA cells following exposure to either PR-104A or SN34507 (0.05 μM) under aerobic conditions.

Please cite this article in press as: A.M. Mowday et al., Rational design of an AKR1C3-resistant analog of PR-104 for enzyme-prodrug therapy, Biochem. Pharmacol. (2016), http://dx.doi.org/10.1016/j.bcp.2016.07.015

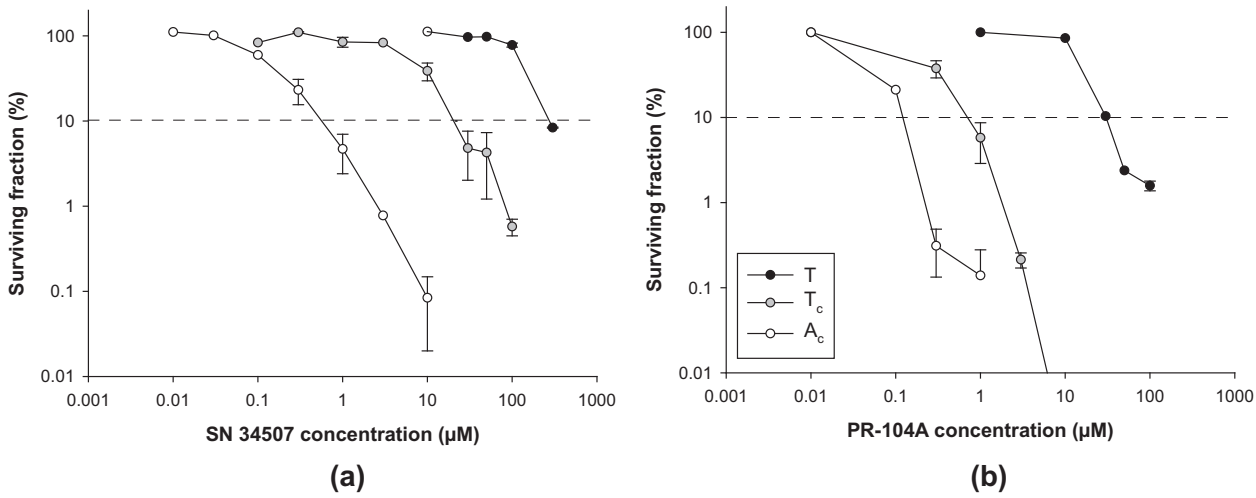

Fig. 7. *E. coli* NfsA-dependent bystander effects of SN34507 and PR-104A in tissue-like multicellular cultures: (a) SN34507 dose-dependent clonogenic killing of NfsA-positive 'activator' (A_c) cells (○), WT 'target' (T) cells (●) and target cells (T_c) in the presence of 3% activators (●) under hyperoxic conditions; (b) PR-104A dose-dependent clonogenic killing of NfsA-positive 'activator' (A_c) cells (○), WT 'target' (T) cells (●) and target cells (T_c) in the presence of 3% activators (●) under hyperoxic conditions. Data are the average of three independent experiments ± SD.

As expected, tumors lacking NfsA-expressing cells (100% WT tumors) displayed minimal sensitivity to either prodrug, with a non-significant increase in median survival for either agent ($P = 0.90$, Log-rank test). Mixed tumors composed of 30% NfsA/70% WT cells (±4.4% as determined by ex-vivo expression analysis) were sensitive to both agents. Treatment with PR-104 increased median survival by 8 days, with a tumor growth delay of 150% ($P < 0.001$, Log-rank test). Treatment with SN35539 provided a 325% tumor growth delay ($P < 0.001$, Log-rank test), with gain in median survival being significantly greater than PR-104 treated tumors (8 vs 26 days, $P < 0.001$, Log-rank test). The body weight loss associated with each treatment was minimal (<10% of pre-treatment weight, data not shown).

4. Discussion

An ideal GDEPT prodrug is substantially less cytotoxic than its corresponding active metabolite(s) and is a unique substrate for the chosen prodrug activating enzyme under physiological conditions. PR-104 is a clinical stage nitroaromatic prodrug that is demonstrably more active than the prototypical NTR prodrug CB1954 in gene therapy models [24]. Nevertheless, several mechanisms of PR-104A activation including hypoxia-selective metabolism [10], aerobic activation by AKR1C3 [15] and oxygen-insensitive non-CYP450 hepatic enzymes [36], indicate this prodrug lacks selectivity for NTRs in the systemic setting. In order to generate an NTR-specific prodrug for gene therapy applications, the chemical structure of PR-104A was modified to minimize activation by endogenous human enzymes. Rational design led to the synthesis of the prodrug SN34507, an analog of PR-104A lacking the ancillary *ortho* nitro moiety predicted to reduce recognition by the AKR1C3 active site. Additionally, the potential for *ortho* nitro reduction leading to intramolecular cyclization of the activate metabolite to form non-cytotoxic by-products (as seen for PR-104A [10]) is negated. Loss of AKR1C3-dependent cytotoxicity was confirmed in 2D anti-proliferative IC_{50} assays, 3D multicellular layer assays and tumor bearing murine models (Fig. 3). Suggestion of residual activity in low cell density assays did not result in biologically meaningful activity in high cell density MCL and tumor models, with no evidence of AKR1C3 driven antitumor activity.

Removal of the electron withdrawing *ortho* nitro group on the PR-104A scaffold lowered the one-electron reduction potential ($E(1)$) of the remaining *para* nitro 'switch' to −503 ± 10 mV for SN34507. This value indicates net reductive metabolism by one-electron oxidoreductases under anoxic conditions will be minimal as single-electron transfer to SN34507 is not thermodynamically favorable [37]. This was confirmed by the absence of hypoxia-selective cytotoxicity for SN34507 (Fig. 4a) and the minimal influence of high level POR expression (Fig. 4b). In contrast, the more electron affinic substrate PR-104A ($E(1) = -366$ mV) is a known substrate for one-electron oxidoreductases such as cytochrome P450 oxidoreductase (POR) [11].

Following the generation of an analog of PR-104A resistant to reduction by key human one- and two-electron reductases, an optimal bacterial NTR needed to be identified that could activate SN34507. We utilized a library of bacterial nitroreductases expressed in a modified *E. coli* reporter strain to probe for active enzymes that would yield DNA damaging species following exposure to SN34507 [21]. Twenty-five enzymes (44%) from the 58 member NTR library catalyzed a DNA damage-mediated 'SOS response' after exposure to SN34507; all were members of the NfsA or NfsB families. The proportion of active NTRs was lower than seen historically for PR-104A (72%; 34 of 47 active NTRs), which was also a prodrug substrate for AzoR and MdaB family members [21]. Following measurement of the steady state kinetic parameters, the major NTR from *E. coli* NfsA was selected as the preferred bacterial NTR for SN34507 bioactivation. *E. coli* NfsA has previously been identified as a prodrug activating enzyme for the prototypical NTR prodrug CB1954 [33,38,39], and PR-104A [21]. Expression of *E. coli* NfsA in HCT116 colon carcinoma cells confirmed the activation of prodrug SN34507 leading to loss of proliferative potential mediated through a G2/M cell cycle block, as reported for PR-104A (Fig. 6). These data are consistent with the conclusion that the mechanism of action of SN34507 is analogous to PR-104A, with DNA inter-strand crosslink formation giving rise to replication arrest as a consequence of stalled replication forks [14].

In high cell-density (3D) culture models, SN34507 generated a respectable bystander effect (38% efficiency) and exhibited a 464-fold differential in clonogenic cell kill (C_{10}) between activator and target cell populations (T/Ac; Fig. 7a). While PR-104A demonstrated a bystander effect approaching twice that of SN34507 (BEE of 68%) this was associated with poorer selectivity for NfsA-positive cells (T/Ac C_{10} ratio of 250). Of note, PR-104A is more lipophilic than SN34507, a physiochemical property associated

Please cite this article in press as: A.M. Mowday et al., Rational design of an AKR1C3-resistant analog of PR-104 for enzyme-prodrug therapy, Biochem. Pharmacol. (2016), http://dx.doi.org/10.1016/j.bcp.2016.07.015

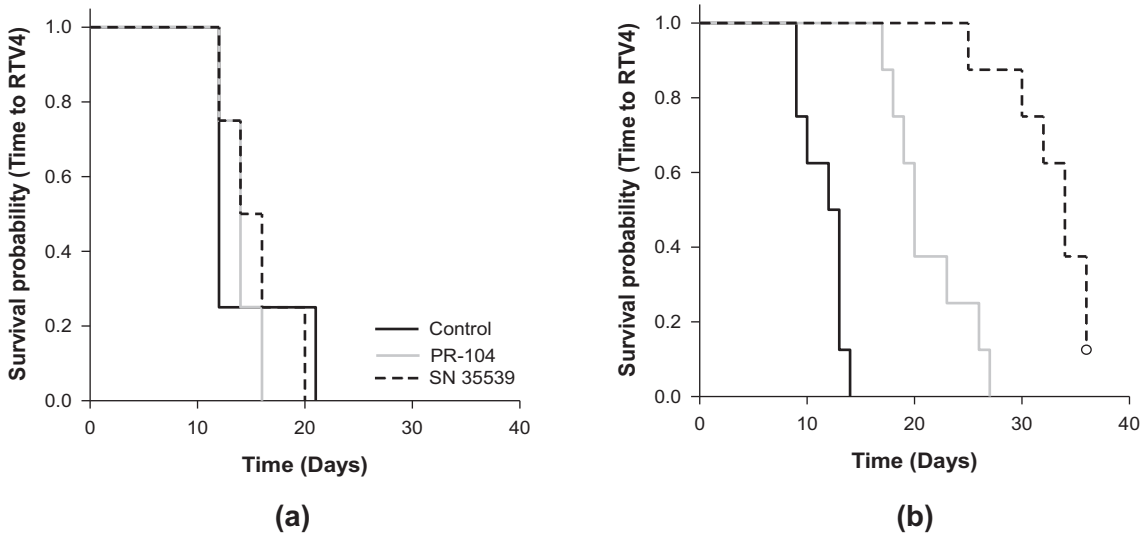

Fig. 8. Relative anti-tumor efficacy of PR-104 and SN35539: (a) 100% HCT116 WT tumor xenografts were treated with a single intraperitoneal dose of vehicle, PR-104 or SN35539 and tumor volume was monitored trice weekly until volume exceeded 4× volume on day of prodrug administration. N = 4 tumors per treatment group; (b) HCT116 xenografts harboring 30% NfsA-positive cells were treated with a single intraperitoneal dose of vehicle, PR-104 or SN35539 and tumor volume was monitored thrice weekly until volume exceeded 4× volume on day of prodrug administration. N = 8 tumors per treatment group. Log-rank test was employed to compare the survival distributions of any two groups.

with improved bystander efficiency [32,35]. However, lipophilicity ($LogD_{7.4}$) is a fundamental characteristic that influences multiple properties of pharmaceutical agents including absorption, distribution, metabolism, excretion and toxicology (ADMET), with less lipophilic compounds typically possessing more favorable ADMET properties [40–42]. In addition to the consideration of their relative partition-coefficients, the major reduced metabolites of PR-104A are predicted to be less reactive than those of SN34507 (due to the presence of the additional electron withdrawing nitro group) and thus are anticipated to diffuse further.

NfsA-dependent SN34507 potency and bystander effect arising from the diffusion of activated metabolites can only partially define the therapeutic utility of a GDEPT prodrug. Overall anti-tumor activity will also depend on the efficiency of metabolic activation at tolerated prodrug doses, determined in part by host toxicokinetics. The original pre-clinical testing of PR-104 was conducted in murine, rat and dog models [10,20], which lack a functional AKR1C3 ortholog capable of activating PR-104A [43]. This evolutionary divergence underlies the non-predictive nature of preclinical toxicology models with respect to PR-104 toxicology in humans (Abbattista, Guise et al., manuscript in preparation). Consequently, when evaluating efficacy in the 'mixed' NfsA/WT xenograft model PR-104 was administered at the "human equivalent dose" (HED) which provides a murine plasma exposure of PR-104A identical to that achieved in human Phase I clinical trials. While the achievable plasma exposure of SN34507 in humans, following administration of SN35539, is currently unknown, it is reasoned that the murine MTD will be representative of the human MTD, since SN34507 is not subject to extensive activation by endogenous reductases, the major source of toxicokinetic discrepancy between species. Consistent with this rationale, the (non-bioreductive) nitrogen mustard melphalan (L-PAM) achieves equivalent plasma exposure in murine and human subjects at their respective maximum tolerated doses [44]. Treatment with SN35539 significantly increased median survival over both control and PR-104 treated tumors ($P < 0.001$, Log-rank test), indicating adequate prodrug penetration, metabolism and subsequent metabolite redistribution sufficient to eliminate the majority of NfsA naïve cells. Single-dose PR-104 displayed modest NfsA-dependent anti-tumor activity compared to untreated control tumors ($P < 0.001$, Log-rank test), but the possibility of activity attributable to one-electron reductases or induction of AKR1C3 activity cannot be excluded.

This study identifies the suicide gene/prodrug partnership of *E. coli* NfsA/SN35539 (SN34507) as a promising combination for development in virus-directed enzyme/prodrug therapy (VDEPT) or bacteria-directed enzyme/prodrug therapy (BDEPT). The inclusion of prodrug activating capability in tumor-tropic replicating vectors can enhance the ability to directly kill cancer cells as demonstrated with *E. coli* NfsB/SN28343 for VDEPT [22] and *E. coli* NfsB/PR-104 for CDEPT [24]. Of significant interest is the potential of armed replicating vectors as immunotherapy enhancing agents. Examples include the recent FDA approval of the HSV-1 derived product talimogene laherparepvec (T-VEC) in unresected stage IIIB/IV melanoma. Tumor-targeted prodrug mediated cell death should enhance vector derived danger signals, providing a more efficient antitumor immune response [45]. There is a need for highly selective suicide gene/prodrug combinations suitable for application in this context. Eliminating off-target enzyme activities associated with endogenous activation of the clinical stage prodrug analog PR-104 has provided the novel prodrug SN35539, suitable for combination with *E. coli* NfsA to achieve much greater systemic selectivity.

Author contributions

AMM, AA, JUF, CPG, DFA, JBS, and AVP conceived and designed the experiments; AMM, AA, EMW, JNC, SS, MRB, MRA and RFA performed the experiments; AMM, JNC, SS, JUF, CPG, JBS and AVP analyzed the data; JNC, DFA, JUF, SS, RFA, CPG, JBS and AVP contributed reagents/materials/analysis tools; AMM, AA, JUF, CPG, JBS and AVP wrote the paper.

Conflicts of interest

The authors declare no conflict of interest. The funders had no role in the study design, collection, analysis and interpretation of data; nor in the writing of the article or the decision to submit the work for publication.

Please cite this article in press as: A.M. Mowday et al., Rational design of an AKR1C3-resistant analog of PR-104 for enzyme-prodrug therapy, Biochem. Pharmacol. (2016), http://dx.doi.org/10.1016/j.bcp.2016.07.015

Acknowledgments

This work was funded by the Health Research Council of New Zealand (Grant 11/1103 and 14/289) and by scholarships from the University of Auckland (awarded to AMM) and the Tertiary Education Commission (a Top Achievers Doctoral award to EMW).

References

[1] G.U. Dachs, M.A. Hunt, S. Syddall, D.C. Singleton, A.V. Patterson, Bystander or no bystander for gene directed enzyme prodrug therapy, Molecules 14 (2009) 4517–4545.
[2] E.M. Williams, R.F. Little, A.M. Mowday, M.H. Rich, J.V. Chan-Hyams, J.N. Copp, et al., Nitroreductase gene-directed enzyme prodrug therapy: insights and advances toward clinical utility, Biochem. J. 471 (2015) 131–153.
[3] I.A. McNeish, N.K. Green, M.G. Gilligan, M.J. Ford, V. Mautner, L.S. Young, et al., Virus directed enzyme prodrug therapy for ovarian and pancreatic cancer using retrovirally delivered *E. coli* nitroreductase and CB1954, Gene Ther. 5 (1998) 1061–1069.
[4] F. Friedlos, S. Court, M. Ford, W.A. Denny, C. Springer, Gene-directed enzyme prodrug therapy: quantitative bystander cytotoxicity and DNA damage induced by CB1954 in cells expressing bacterial nitroreductase, Gene Ther. 5 (1998) 105–112.
[5] J.I. Grove, P.F. Searle, S.J. Weedon, N.K. Green, I.A. McNeish, D.J. Kerr, Virus-directed enzyme prodrug therapy using CB1954, Anticancer Drug Des. 14 (1999) 461–472.
[6] A.H. Djeha, A. Hulme, M.T. Dexter, A. Mountain, L.S. Young, P.F. Searle, et al., Expression of *Escherichia coli* B nitroreductase in established human tumor xenografts in mice results in potent antitumoral and bystander effects upon systemic administration of the prodrug CB1954, Cancer Gene Ther. 7 (2000) 721–731.
[7] G. Chung-Faye, D. Palmer, D. Anderson, J. Clark, M. Downes, J. Baddeley, et al., Virus-directed, enzyme prodrug therapy with nitroimidazole reductase: a phase I and pharmacokinetic study of its prodrug, CB1954, Clin. Cancer Res. 7 (2001) 2662–2668.
[8] G.M. Anlezark, R.G. Melton, R.F. Sherwood, B. Coles, F. Friedlos, R.J. Knox, The bioactivation of 5-(aziridin-1-yl)-2,4-dinitrobenzamide (CB1954) – I. Purification and properties of a nitroreductase enzyme from *Escherichia coli* – a potential enzyme for antibody-directed enzyme prodrug therapy (ADEPT), Biochem. Pharmacol. 44 (1992) 2289–2295.
[9] M.H. Tang, N.A. Helsby, W.R. Wilson, M.D. Tingle, Aerobic 2- and 4-nitroreduction of CB 1954 by human liver, Toxicology 216 (2005) 129–139.
[10] A.V. Patterson, D.M. Ferry, S.J. Edmunds, Y. Gu, R.S. Singleton, K. Patel, et al., Mechanism of action and preclinical antitumor activity of the novel hypoxia-activated DNA crosslinking agent PR-104, Clin. Cancer Res. 13 (2007) 3922–3932.
[11] C.P. Guise, A. Wang, A. Thiel, D. Bridewell, W.R. Wilson, A.V. Patterson, Identification of human reductases that activate the dinitrobenzamide mustard prodrug PR-104A: a role for NADPH:cytochrome P450 oxidoreductase under hypoxia, Biochem. Pharmacol. 74 (2007) 810–820.
[12] C.P. Guise, M.R. Abbattista, S.R. Tipparaju, N.K. Lambie, J. Su, D. Li, et al., Diflavin oxidoreductases activate the bioreductive prodrug PR-104A under hypoxia, Mol. Pharmacol. 81 (2012) 31–40.
[13] Y. Gu, A.V. Patterson, G.J. Atwell, S.B. Chernikova, J.M. Brown, L.H. Thompson, et al., Roles of DNA repair and reductase activity in the cytotoxicity of the hypoxia-activated dinitrobenzamide mustard PR-104A, Mol. Cancer Ther. 8 (2009) 1714–1723.
[14] R.S. Singleton, C.P. Guise, D.M. Ferry, S.M. Pullen, M.J. Dorie, J.M. Brown, et al., DNA crosslinks in human tumor cells exposed to the prodrug PR-104A: relationships to hypoxia, bioreductive metabolism and cytotoxicity, Cancer Res. 69 (2009) 3884–3891.
[15] C.P. Guise, M. Abbattista, R.S. Singleton, S.D. Holford, J. Connolly, G.U. Dachs, et al., The bioreductive prodrug PR-104A is activated under aerobic conditions by human aldo-keto reductase 1C3, Cancer Res. 70 (2010) 1573–1584.
[16] Y. Jin, T.M. Penning, Aldo-keto reductases and bioactivation/detoxication, Annu. Rev. Pharmacol. Toxicol. 47 (2007) 263–292.
[17] J. Birtwistle, R.E. Hayden, F.L. Khanim, R.M. Green, C. Pearce, N.J. Davies, et al., The aldo-keto reductase AKR1C3 contributes to 7,12-dimethylbenz(a) anthracene-3,4-dihydrodiol mediated oxidative DNA damage in myeloid cells: implications for leukemogenesis, Mutat. Res. 662 (2009) 67–74.
[18] M.B. Jameson, D. Rischin, M. Pegram, J. Gutheil, A.V. Patterson, W.A. Denny, et al., A phase I trial of PR-104, a nitrogen mustard prodrug activated by both hypoxia and aldo-keto reductase 1C3, in patients with solid tumors, Cancer Chemother. Pharmacol. 65 (2010) 791–801.
[19] M.J. McKeage, Y. Gu, W.R. Wilson, A. Hill, K. Amies, T.J. Melink, et al., A phase I trial of PR-104, a pre-prodrug of the bioreductive prodrug PR-104A, given weekly to solid tumour patients, BMC Cancer 11 (2011) 432.
[20] K. Patel, S.F. Choy, K.O. Hicks, T.J. Melink, N.H.G. Holford, W.R. Wilson, A combined pharmacokinetic model for the hypoxia-targeted prodrug PR-104A in humans, dogs, rats and mice predicts species differences in clearance and toxicity, Cancer Chemother. Pharmacol. 67 (2011) 1145–1155.
[21] G.A. Prosser, J.N. Copp, A.M. Mowday, C.P. Guise, S.P. Syddall, E.M. Williams, et al., Creation and screening of a multi-family bacterial oxidoreductase library to discover novel nitroreductases that efficiently activate the bioreductive prodrugs CB1954 and PR-104A, Biochem. Pharmacol. 85 (2013) 1091–1103.
[22] D.C. Singleton, D. Li, S.Y. Bai, S.P. Syddall, J.B. Smaill, Y. Shen, et al., The nitroreductase prodrug SN 28343 enhances the potency of systemically administered armed oncolytic adenovirus ONYX-411(NTR), Cancer Gene Ther. 14 (2007) 953–967.
[23] W.R. Wilson, K.O. Hicks, S.M. Pullen, D.M. Ferry, N.A. Helsby, A.V. Patterson, Bystander effects of bioreductive drugs: potential for exploiting pathological tumor hypoxia with dinitrobenzamide mustards, Radiat. Res. 167 (2007) 625–636.
[24] S.C. Liu, G.O. Ahn, M. Kioi, M.J. Dorie, A.V. Patterson, J.M. Brown, Optimised clostridium-directed enzyme prodrug therapy improves the antitumor activity of the novel DNA crosslinking agent PR-104, Cancer Res. 68 (2008) 7995–8003.
[25] G.E. Adams, E.D. Clarke, R.S. Jacobs, I.J. Stratford, R.G. Wallace, P. Wardman, et al., Mammalian cell toxicity of nitro compounds: dependence upon reduction potential, Biochem. Biophys. Res. Commun. 72 (1976) 824–829.
[26] S.M. Bailey, R.J. Knox, S.M. Hobbs, T.C. Jenkins, A.B. Mauger, R.G. Melton, et al., Investigation of alternative prodrugs for use with *E. coli* nitroreductase in 'suicide gene' approaches to cancer therapy, Gene Ther. 3 (1996) 1143–1150.
[27] S. Yang, G.J. Atwell, W.A. Denny, Synthesis of asymmetric halomesylate mustards with aziridineethanol/alkali metal halides: application to an improved synthesis of the hypoxia prodrug PR-104, Tetrahedron 63 (2007) 5470–5476.
[28] G.J. Atwell, W.A. Denny, Synthesis of ^{3}H- and $^{2}H_{4}$-labelled versions of the hypoxia-activated pre-prodrug 2-[(2-bromoethyl)-2,4-dinitro-6-[[[2-(phosphonooxy)ethyl]amino]carbonyl]anilino]ethyl methanesulfonate (PR-104), J. Labelled Comp. Radiopharm. 50 (2007) 7–12.
[29] J.U. Flanagan, G.J. Atwell, D.M. Heinrich, D.G. Brooke, S. Silva, L.J. Rigoreau, et al., Morpholylureas are a new class of potent and selective inhibitors of the type 5 17-b-hydroxysteroid dehydrogenase (AKR1C3), Bioorg. Med. Chem. 22 (2014) 967–977.
[30] M.L. Verdonk, J.C. Cole, M.J. Hartshorn, C.W. Murray, R.D. Taylor, Improved protein-ligand docking using GOLD, Proteins 52 (2003) 609–623.
[31] N.A. Helsby, G.J. Atwell, S. Yang, B.D. Palmer, R.F. Anderson, S.M. Pullen, et al., Aziridinyldinitrobenzamides: synthesis and structure-activity relationships for activation by *E. coli* nitroreductase, J. Med. Chem. 47 (2004) 3295–3307.
[32] W.R. Wilson, S.M. Pullen, A. Hogg, N.A. Helsby, K.O. Hicks, W.A. Denny, Quantitation of bystander effects in nitroreductase suicide gene therapy using three-dimensional cell cultures, Cancer Res. 62 (2002) 1425–1432.
[33] G.A. Prosser, J.N. Copp, S.P. Syddall, E.M. William, J.B. Smaill, W.R. Wilson, et al., Discovery and evaluation of *Escherichia coli* nitroreductases that activate the anticancer prodrug CB 1954, Biochem. Pharmacol. 79 (2010) 678–687.
[34] A.L. Lovering, J.P. Ride, C.M. Bunce, J.C. Desmond, S.M. Cummings, S.A. White, Crystal structures of prostaglandin D(2) 11-ketoreductase (AKR1C3) in complex with the nonsteroidal anti-inflammatory drugs flufenamic acid and indomethacin, Cancer Res. 64 (2004) 1802–1810.
[35] G.J. Atwell, S. Yang, F.B. Pruijn, S.M. Pullen, A. Hogg, A.V. Patterson, et al., Synthesis and structure-activity relationships for 2,4-dinitrobenzamide-5 mustards as prodrugs for the *Escherichia coli nfsB* nitroreductase in gene therapy, J. Med. Chem. 50 (2007) 1197–1212.
[36] Y. Gu, C.P. Guise, K. Patel, M.R. Abbattista, J. Li, X. Sun, et al., Reductive metabolism of the dinitrobenzamide mustard anticancer prodrug PR-104 in mice, Cancer Chemother. Pharmacol. 67 (2011) 543–555.
[37] P. Wardman, M.F. Dennis, S.A. Everett, K.B. Patel, M.R. Stratford, M. Tracy, Radicals from one-electron reduction of nitro compounds, aromatic N-oxides and quinones: the kinetic basis for hypoxia-selective, bioreductive drugs, Biochem. Soc. Symp. 61 (1995) 171–194.
[38] S.O. Vass, D. Jarrom, W.R. Wilson, E.I. Hyde, P.F.E. Searle, Coli NfsA: an alternative nitroreductase for prodrug activation gene therapy in combination with CB1954, Br. J. Cancer 100 (2009) 1903–1911.
[39] Y. Barak, S.H. Thorne, D.F. Ackerley, S.V. Lynch, C.H. Contag, A. Matin, New enzyme for reductive cancer chemotherapy, YieF, and its improvement by directed evolution, Mol. Cancer Ther. 5 (2006) 97–103.
[40] P.D. Leeson, B. Springthorpe, The influence of drug-like concepts on decision-making in medicinal chemistry, Nat. Rev. Drug Discov. 6 (2007) 881–890.
[41] J.D. Hughes, J. Blagg, D.A. Price, S. Bailey, G.A. Decrescenzo, R.V. Devraj, et al., Physiochemical drug properties associated with in vivo toxicological outcomes, Bioorg. Med. Chem. Lett. 18 (2008) 4872–4875.
[42] J.A. Arnott, S.L. Planey, The influence of lipophilicity in drug discovery and design, Expert Opin. Drug Discov. 7 (2012) 863–875.
[43] P. Velica, N.J. Davies, P.P. Rocha, H. Schrewe, J.P. Ride, C.M. Bunce, Lack of functional and expression homology between human and mouse aldo-keto reductase 1C enzymes: implications for modelling human cancers, Mol. Cancer 8 (2009) 121–132.
[44] J.K. Peterson, P.J. Houghton, Integrating pharmacology and in vivo cancer models in preclinical and clinical drug development, Eur. J. Cancer 40 (2004) 837–844.
[45] H.L. Kaufman, F.J. Kohlhapp, A. Zloza, Oncolytic viruses: a new class of immunotherapy drugs, Nat. Rev. Drug Discov. 14 (2015) 642–662.

Please cite this article in press as: A.M. Mowday et al., Rational design of an AKR1C3-resistant analog of PR-104 for enzyme-prodrug therapy, Biochem. Pharmacol. (2016), http://dx.doi.org/10.1016/j.bcp.2016.07.015